This article has been accepted for publication in a future issue of this journal, but has not been fully edited. Content may change prior to final publication. Citation information: DOI 10.1109/TIE.2018.2847661, IEEE Transactions on Industrial Electronics

A Complex Repetitive Controller Based on the Generalized Delayed Signal Cancelation Method

Felipe J. Zimann, *Student Member, IEEE,* Rafael C. Neto, Francisco A. S. Neves, *Senior Member, IEEE,* Helber E. P. de Souza, Alessandro L. Batschauer, *Member, IEEE,* and Cassiano Rech, *Senior Member, IEEE*

***Abstract*—In this paper, a generic complex repetitive controller ($nk + m$ RC, $k \in \mathbb{Z}$), based on the inverse transfer function of the generalized delayed signal cancelation transformation is proposed. The presented complex controller can be designed for regulating different positive- and negative-sequence harmonic components through a space-vector error signal, with improved response time as compared to traditional repetitive controllers. An evaluation of the proposed control scheme stability, based on phase margin, Nyquist diagram and sensitivity function is presented. The effects of the controller parameters on the system's stability and also on its dynamic response are shown and allow the definition of some control design guidelines. Experimental results are presented to validate the theoretical assumptions through applying the proposed controller for regulating the currents in a three-phase active power filter.**

***Index Terms*—Harmonic compensation, repetitive control, complex controller, active power filter.**

NOMENCLATURE

APF	Active Power Filter
CRC	Conventional Repetitive Controller
FFPS	Fundamental-Frequency Positive-Sequence
GDSC	Generalized Delayed Signal Cancelation
iGDSC	Inverse Transfer Function of the GDSC
OLTF	Open-Loop Transfer Function
RC	Repetitive Controller
SV-RC	Space-Vector Repetitive Controller
VTHD	Vector Total Harmonic Distortion

Manuscript received Month xx, 2xxx; revised Month xx, xxxx; accepted Month x, xxxx. This work was developed with the support of the *Programa Nacional de Cooperação Acadêmica da Coordenação de Aperfeiçoamento de Pessoal de Nível Superior* – CAPES/Brazil. The authors would like to thank CNPq, INCT-GD, CAPES (process 23038.000776/2017-54), UDESC, FAPESC, FACEPE and FAPERGS (process 17/2551-0000517-1), for the financial support.

F. J. Zimann and A. L. Batschauer are with the Department of Electrical Engineering, *Universidade do Estado de Santa Catarina*, Joinville, 89219-710, Brazil (e-mail: felipezimann@ieee.org; alessandro.batschauer@udesc.br).

R. C. Neto and F. A. S. Neves are with the Power Electronics and Drives Research Group (GEPAE), DEE, *Universidade Federal de Pernambuco*, Recife, 50740-530, Brazil (e-mail: rafael.cavalcantineto@ufpe.br; fneves@ufpe.br).

H. E. P. de Souza is with the Department of Industry, *Instituto Federal de Educação, Ciência e Tecnologia de Pernambuco*, Pesqueira, 50740-540, Brazil (e-mail: helberelias@pesqueira.ifpe.edu.br).

C. Rech is with the Power Electronics and Control Research Group (GEPOC), *Universidade Federal de Santa Maria*, Santa Maria, 97105-900, Brazil (e-mail: rech.cassiano@gmail.com).

Digital Object Identifier XXXXXXXXXXXXXXXXXXXXXXXXX

I. INTRODUCTION

IN ORDER TO DESIGN A CONTROL SYSTEM, it is advisable to recognize the performance requirements. Also, it is useful to know the plant model and the characteristics of the reference signals for the choice of the most appropriate control strategy.

When the reference signals are periodic, many possible solutions are proposed in the literature [1] - [9]. In three-phase grid-connected converters, it is often necessary to use controllers capable of imposing not only fundamental-frequency positive-sequence (FFPS) reference signals, but also signals containing negative-sequence and harmonic components.

In order to perform these tasks, the first technique proposed was based on proportional + integral (PI) controllers implemented on the d and q axes of a dq rotating reference-frame oriented by the voltage vector at the point of common coupling (PCC) [1] [2]. In this oriented reference frame, the d and q components of a three-phase balanced sinusoidal signal become constant. For this reason, the PI controllers allow for the achievement of good performance for the FFPS component. However, negative-sequence or harmonic components are not adequately imposed, since magnitude and phase errors are expected. This problem can be overcome if multiple PI controllers are used, implemented in multiple rotating reference-frames [3]. However, this would require several rotational transformations, increasing the complexity of the control scheme.

The many rotational transformations can be avoided by using proportional + resonant (P-RES) controllers in parallel [4]. For doing so, one can use a set of P-RES controllers for each phase quantity (a, b and c) or transform the errors to $\alpha\beta$ reference-frame and use sets of P-RES controllers in the α and β components. One second-order resonant controller, also named second-order generalized integrator (SOGI) [5] or proportional with sinusoidal signal integrator (P-SSI) [6], ensures zero steady-state error for the pair of frequencies $\pm\omega_0$, where ω_0 is the resonance frequency and the negative signal means negative-sequence. It is possible to ensure zero steady-state error for only one specific sequence component by using a complex controller, such as the reduced-order generalized integrator (ROGI) [7] or the controller based on the space-vector Fourier transform (SVFT-based controller) [8].

In usual applications, it is necessary to control three-phase signals that contain the fundamental component and a typical set of harmonic components, for example $(6k \pm 1, k \in \mathbb{N})$.

0278-0046 (c) 2018 IEEE. Personal use is permitted, but republication/redistribution requires IEEE permission. See http://www.ieee.org/publications_standards/publications/rights/index.html for more information.

This article has been accepted for publication in a future issue of this journal, but has not been fully edited. Content may change prior to final publication. Citation information: DOI 10.1109/TIE.2018.2847661, IEEE Transactions on Industrial Electronics

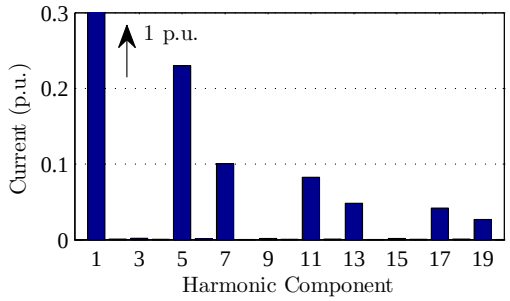

Figure 1. Harmonic spectrum of the phase current of a three-phase rectifier.

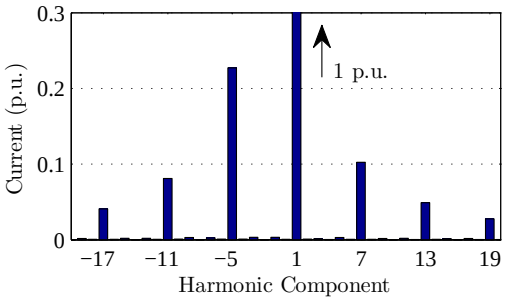

Figure 2. Harmonic spectrum of the space-vector of a three-phase rectifier input current.

In these cases, it is useful to transform the error signals to synchronous reference-frame and implement SOGI controllers in parallel tuned in the harmonic components ($6k$, $k \in \mathbb{N}$). The SOGI controller for $k = 0$ performs the integral action necessary for regulating the FFPS component.

In the cases where a set of harmonic components must be controlled, an interesting alternative is the use of repetitive controllers (RC) [9] [10]. Conventional RC (CRC) are capable of regulating, with zero steady-state error, all harmonic components. In order to implement this controller, all samples of the error signal during the last period must be stored. However, the reference signals generally do not contain all harmonic components. Thus, designing the controller to compensate only the necessary harmonic components leads to the reduction of the number of stored samples and, consequently, a faster response [11]. RCs for regulating families of harmonic components of the type ($4k\pm1$, $k \in \mathbb{N}$) (all odd components) [12] and ($6k\pm1$, $k \in \mathbb{N}$) [13] were then proposed.

A typical example of the usefulness of these RCs occurs when the harmonic current components of a three-phase rectifier must be compensated using a shunt active power filter (APF). The phase currents in this case have all harmonic components of the family ($6k \pm 1$, $k \in \mathbb{N}$). Fig. 1 shows the harmonic spectrum of the phase a current measured in a three-phase rectifier input. The currents of phases b and c have this same harmonic spectrum. However, the harmonic components of order $6k - 1$ have negative-sequence ($a - c - b$), while those of order $6k + 1$ have positive-sequence ($a - b - c$). This fact can be confirmed observing the harmonic spectrum of the three-phase currents' space-vector, obtained through the Clarke transform. Consider, for example, a three-phase harmonic component of a negative-sequence signal:

$$\begin{cases} i_a^h = I_h \cos(h\omega t) \\ i_b^h = I_h \cos(h\omega t + \frac{2\pi}{3}) \\ i_c^h = I_h \cos(h\omega t - \frac{2\pi}{3}) \end{cases} . \quad (1)$$

The corresponding space-vector is $\vec{i}_h = I_h e^{-jh\omega t}$. If this three-phase signal had positive-sequence, the space-vector would be $\vec{i}_h = I_h e^{jh\omega t}$. Thus, one can plot the harmonic spectrum of the three-phase signal space-vector, for distinguishing between the harmonic components of positive-sequence ($a - b - c$) and negative-sequence ($a - c - b$). Fig. 2 shows the harmonic spectrum of the space-vector obtained from the three-phase rectifier measured currents, confirming the different families of negative-sequence and positive-sequence harmonic components. Then, one can say that the harmonic spectrum of the three-phase rectifier currents' space-vector has components in the family $h = 6k + 1$, observing that now $k \in \mathbb{Z}$, where the negative harmonics indicate negative-sequence components.

A generic order repetitive controller ($nk \pm m$ RC, $k \in \mathbb{N}$) was proposed in [14] [11]. Two independent RCs are applied to the α and β components separately. For this reason, the results are equivalent to applying them to the phase a, b and c quantities, and the controller has poles on the harmonic components of order ($\pm(nk \pm m)$, $k \in \mathbb{N}$), i. e., it always regulates the positive- and negative-sequence harmonic components of the same order. Thus, the order of these controllers, when compared with their application to a space-vector, may be superior to the necessary order.

The proposal of a complex RC applied to the space-vector of the error signal, or space-vector repetitive controller (SV-RC), provides the ability to regulate harmonic components of order ($nk + m$, $k \in \mathbb{Z}$). In other words, the frequencies of the positive-sequence regulated components are different from those of negative-sequence regulated components. Its application to the example above would allow regulating only the necessary harmonic components, reducing the controller order, the number of samples stored and the response time. In fact, in order to implement the $6k \pm 1$ RC for regulating the harmonic components in a three-phase PWM inverter, the maximum time delay in the forward channel is $N/3$ [11], with N being the number of samples per fundamental period. In the case of using a SV-RC, the current sample and the one delayed $N/6$ are used, making the controller action faster.

In this paper, a generic SV-RC, based on the inverse transfer function of the generalized delayed signal cancelation (GDSC) transformation is proposed ($nk+m$ RC, $k \in \mathbb{Z}$). Different possible configurations are presented and compared. Furthermore, a design methodology is presented. Recently, a complex RC sensitive to phase sequence was proposed [15], which has been shown to be equivalent to one of the configurations proposed in this article. From the stability analysis presented, the structure proposed here, later called iGDSC, has shown better stability properties in comparison with the one presented in [15].

The paper is organized as follows: Section II presents the fundamentals of the proposed SV-RC and a comparison between this controller and other RC-based solutions. An evaluation of the proposed SV-RC's stability and design methodology, based on phase margin, Nyquist diagram and

0278-0046 (c) 2018 IEEE. Personal use is permitted, but republication/redistribution requires IEEE permission. See http://www.ieee.org/publications_standards/publications/rights/index.html for more information.

This article has been accepted for publication in a future issue of this journal, but has not been fully edited. Content may change prior to final publication. Citation information: DOI 10.1109/TIE.2018.2847661, IEEE Transactions on Industrial Electronics

sensitivity function are presented in Section III. The presented SV-RC is applied for regulating the currents in a three-phase APF. The results, shown in Section IV, validate the theoretical assumptions and demonstrate the potential of the proposed scheme that uses a unique, fast, precise and very simple controller able to regulate a set of positive- and negative-sequence components of a three-phase signal. Finally, conclusions are presented in Section V.

II. The Proposed GDSC-Based Controller

A. Fundamentals of the GDSC

Looking for a fast and accurate method for obtaining the FFPS component of three-phase signals, the GDSC transformation was proposed in [16]. This transformation consists of a complex mathematical operation designed to be applied to a space-vector. It combines current and delayed samples of the input space-vector $\vec{s}_{\alpha\beta}$ in order to cancel a family of specific harmonic components, as follows:

$$\vec{f}_{gdsc}(iT_s) = \vec{a}\{\vec{s}_{\alpha\beta}(iT_s) + e^{j\theta_r}\vec{s}_{\alpha\beta}[(i-i_d)T_s]\}, \quad (2)$$

where iT_s is the instant of the current sample, i_d defines the delay in number of samples, θ_r is an angle by which the delayed space-vector $\vec{s}_{\alpha\beta}[(i-i_d)T_s]$ is rotated and $\vec{a}$ is a constant complex gain. Alternatively, (2) can be written in the z domain as

$$\vec{f}_{gdsc}(z) = \underbrace{\vec{a}[1+e^{j\theta_r}z^{-i_d}]}_{\vec{G}_{gdsc}}\vec{s}_{\alpha\beta}(z). \quad (3)$$

Since the $h-th$ harmonic component of the delayed space-vector is equal to

$$\vec{s}^{(h)}_{\alpha\beta}[(i-i_d)T_s] = e^{-jh\frac{2\pi}{N}i_d}\vec{s}^{(h)}_{\alpha\beta}(iT_s), \quad (4)$$

then the transformed signal of the $h-th$ harmonic component becomes

$$\vec{f}^{(h)}_{gdsc}(iT_s) = \underbrace{\vec{a}[1+e^{j\theta_r}e^{-jh\frac{2\pi}{N}i_d}]}_{\vec{G}^{(h)}_{gdsc}}\vec{s}^{(h)}_{\alpha\beta}(iT_s), \quad (5)$$

where $\vec{G}^{(h)}_{gdsc}$ is the gain for the $h-th$ harmonic component. Considering a family of harmonic components ($nk+m$, $k\in\mathbb{Z}$), where m is one of the harmonic components with gain equal to zero and n is the periodicity of the eliminated components, the transformation parameters can be determined from

$$i_d = \frac{N}{n} \quad ; \quad \theta_r = \frac{m}{n}2\pi + \pi. \quad (6)$$

The value of $\vec{a}$ is determined for imposing unity gain on the harmonic component to be detected.

The frequency response of the GDSC transformation designed to cancel harmonic components in the family ($6k+1$, $k\in\mathbb{Z}$) can be seen in Fig. 3. The parameters for this transformation are $i_d = N/6$, $\theta_r = 4\pi/3$ and $\vec{a} = 0.5$. From (6) it is clear that the term i_d determines the periodicity of the components with gain equal to zero, while θ_r defines one of those components.

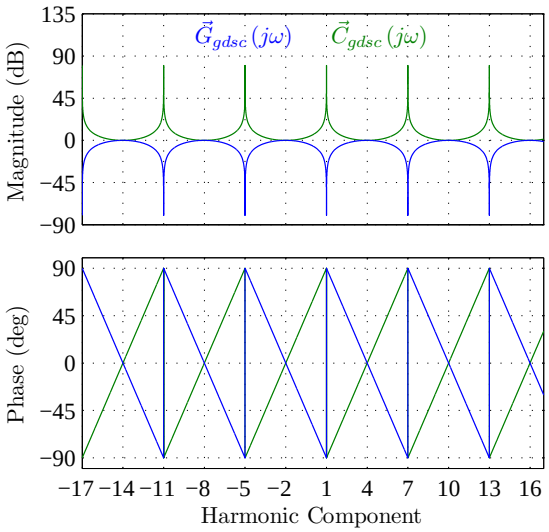

Figure 3. Bode frequency responses of GDSC ($\vec{G}_{gdsc}(j\omega)$) and iGDSC ($\vec{C}_{gdsc}(j\omega)$) transfer functions designed to actuate at the harmonic components ($6k+1$, $k\in\mathbb{Z}$), for $\vec{a}=0.5$.

B. Proposed Controller

According to the internal model principle [17], it is well known that a controller ensures zero steady-state error when tracking a sinusoidal reference signal with frequency ω_1 if the open-loop transfer function (OLTF) has a pole at frequency ω_1 and the closed-loop system is stable.

The inverse transfer function of the GDSC transformation (iGDSC) can be used as a SV-RC for imposing a reference signal containing any harmonic components in the family ($nk+m$, $k\in\mathbb{Z}$), for which the GDSC has gain equal to zero (or minus infinite in dB), as can be observed in Fig. 3. Taking the error space-vector $\vec{e}_{\alpha\beta}$ as controller input and $\vec{u}_{\alpha\beta}$ as its output, the iGDSC controller gain ($\vec{C}_{gdsc}$) must be

$$\vec{C}_{gdsc} = \frac{\vec{u}_{\alpha\beta}}{\vec{e}_{\alpha\beta}} = \frac{1}{\vec{G}_{gdsc}} = \frac{1}{\vec{a}(1+e^{j\theta_r}z^{-i_d})}, \quad (7)$$

and then

$$\vec{u}_{\alpha\beta}[i] = -e^{j\theta_r}\vec{u}_{\alpha\beta}[i-i_d] + \frac{1}{\vec{a}}\vec{e}_{\alpha\beta}[i]. \quad (8)$$

According to (8), the block diagram of the controller in its complex form is the one shown in Fig. 4. Analyzing this block diagram, it can be observed that the proposed controller has a generator of periodic signals implemented in the feedback path.

The choice of the parameters i_d and θ_r is made based on (6), used for the GDSC design. On the other hand, using a real $\vec{a}$ is equivalent to applying a gain $1/\vec{a}$ to the controller, while using a complex $\vec{a}$ affects the gain and also the phase of the controller, having some effect on the system stability. In this article only real $\vec{a}$ was used. The evaluation of a complex parameter $\vec{a}$ was left for future research.

It is important to notice that the block diagram of the iGDSC controller can be implemented using a positive feedback. In fact, since

$$e^{j\theta_r} = e^{j\left(\frac{m}{n}2\pi+\pi\right)} = e^{j\frac{m}{n}2\pi}\cdot e^{j\pi} = -e^{j\frac{m}{n}2\pi}, \quad (9)$$

the block diagram shown in Fig. 4 can be reorganized in order to obtain the one shown in Fig. 5.

0278-0046 (c) 2018 IEEE. Personal use is permitted, but republication/redistribution requires IEEE permission. See http://www.ieee.org/publications_standards/publications/rights/index.html for more information.

This article has been accepted for publication in a future issue of this journal, but has not been fully edited. Content may change prior to final publication. Citation information: DOI 10.1109/TIE.2018.2847661, IEEE Transactions on Industrial Electronics

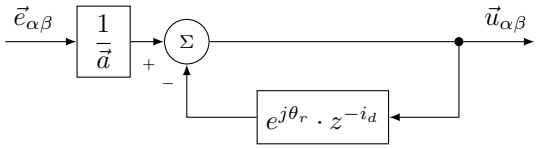

Figure 4. Block diagram of iGDSC controller using complex notation.

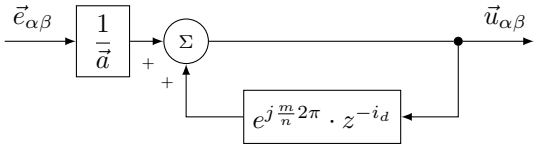

Figure 5. Block diagram of iGDSC controller with positive feedback.

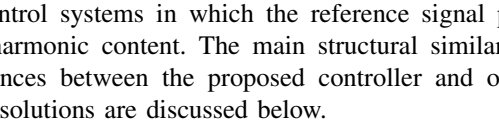

Figure 6. Block diagram of the CRC, presented in [10].

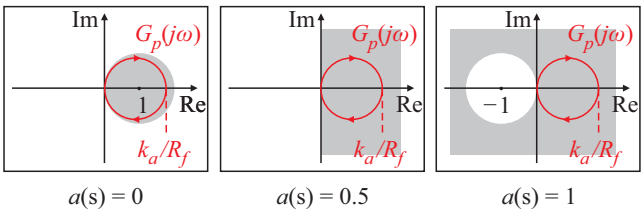

Figure 7. Stability domains for RC systems, according to [18].

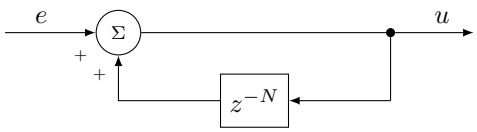

Figure 8. Block diagram of the CRC with $a(s) = 1$ and discretized delay.

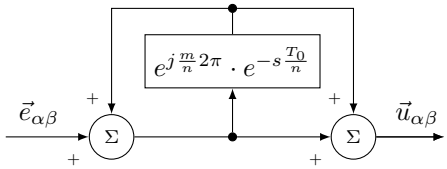

Figure 9. RC structure presented in [15].

C. Structure Comparison Between the Proposed Controller and Other RC-Based Solutions

As presented in Section I, RC-based solutions are suitable for control systems in which the reference signal possesses high harmonic content. The main structural similarities and differences between the proposed controller and other RC-based solutions are discussed below.

1) CRC proposed by Hara et al. [10]: As shown in Fig. 6, the CRC is composed of a periodic signal generator of fundamental cycle T_0 and a gain $a(s)$ in a second direct path.

In [18], it is shown that single-input single-output (SISO) systems using RC with constant $a(s)$ will be stable if the Nyquist diagram of the plant ($G_p(j\omega)$) remains inside of some regions of the complex plan, named stability domains. The choice of the parameter $a(s)$ results in distinct stability domains, as shown in the shaded regions of Fig. 7, in which the Nyquist diagram of a plant with zero relative degree is also plotted. It can be observed that the configuration in which $a(s) = 1$ is less restrictive in terms of plants to which the RC can be applied and, according to Hara et al. [18], it is most appropriate for non-linear systems. In Fig. 8, the block diagram of the CRC with $a(s) = 1$ and discretized delay is shown.

It is important to notice that the proposed controller has a SISO structure, but with complex input and output. By comparing Fig. 5 and Fig. 8, it is possible to observe an important similarity: both controllers have a similar periodic reference generator. The delays (z^{-i_d} and z^{-N}) are implemented in the positive feedback path, so that they have the same stability domains. However, these controllers regulate different families of harmonic components. CRCs have infinite gain in all harmonic components while the iGDSC controller is designed to regulate only those in the family ($nk+m$, $k \in \mathbb{Z}$). Besides the frequency selectivity, the iGDSC controller needs less memory cells and is implemented using a smaller delay, as can be seen in Table I.

2) $nk \pm m$ RC proposed by Lu et al. [11]: For applications that require higher frequency selectivity, several advantages are obtained by using the $nk \pm m$ RC instead of the CRC [11]. This solution makes it possible to regulate reference signals that possess high harmonic content in the family ($nk \pm m$, $k \in \mathbb{N}$).

Since the $nk \pm m$ RC is a real controller, when applied to a three-phase system using a natural abc reference frame, three controllers are necessary for regulating the reference signals. On the other hand, if the $\alpha\beta$ reference frame is used, the number of controllers is reduced to two. For this same application, the SV-RCs are implemented using only one complex controller. Again, as shown in Table I, the SV-RCs (including the iGDSC) require less memory cells and are implemented using a smaller delay.

3) SV-RC proposed by Luo et al. [15]: As presented in Section I, for control systems in which the reference signals can be represented by a space-vector and possess high harmonic content, the SV-RC becomes a viable solution. Luo et al. [15] proposed the SV-RC whose block diagram is shown in Fig. 9. By comparing this diagram with that of the CRC for which $a(s) = 0.5$ (Fig. 10), one can observe the similarity in their periodic signal generator structures, leading to the conclusion that both have the same stability domain. Thus, when compared to the SV-RC presented in [15], the iGDSC has a larger stability domain. In terms of memory cells, due to the complex nature of the structures, both strategies require N/n elements to store the real part and N/n elements for the imaginary part.

It is important to point out that the SV-RC proposed by Luo et al. [15] can be implemented using the GDSC transformation. This can be done by using the block diagram of Fig. 11.

0278-0046 (c) 2018 IEEE. Personal use is permitted, but republication/redistribution requires IEEE permission. See http://www.ieee.org/publications_standards/publications/rights/index.html for more information.

This article has been accepted for publication in a future issue of this journal, but has not been fully edited. Content may change prior to final publication. Citation information: DOI 10.1109/TIE.2018.2847661, IEEE Transactions on Industrial Electronics

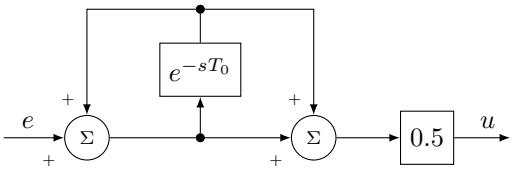

Figure 10. Block diagram of the CRC with $a(s) = 0.5$.

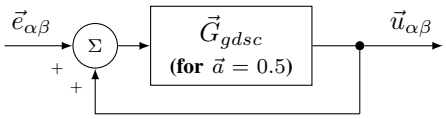

Figure 11. Block diagram of GDSC-based implementation of the SV-RC proposed by Luo et al. [15].

Table I
COMPARISON OF CONTROLLERS' STRUCTURAL CHARACTERISTICS.

Control strategy	Maximum time delay in samples	Total number of memory cells
CRC [10]	N	$N \times NoA^*$
$nk \pm m$ RC [11]	$2 \cdot N/n$	$3 \cdot N/n \times NoA^*$
$nk + m$ SV-RC [15]	N/n	$2 \cdot N/n$
$nk + m$ iGDSC	N/n	$2 \cdot N/n$

* $NoA = 3$ for implementation using abc reference frame;
$NoA = 2$ for implementation using $\alpha\beta$ reference frame.

III. STABILITY ANALYSIS AND DESIGN METHODOLOGY

In order to design the iGDSC controller, the designer must identify the family of harmonic components ($nk + m$, $k \in \mathbb{Z}$) that need to be controlled. This family can be obtained by analyzing the harmonic spectrum of the space-vector reference signal. For the application evaluated in this paper (Fig. 2), these harmonics are in the set ($6k + 1$, $k \in \mathbb{Z}$). Besides that, the plant should be modeled, in order to allow the stability analysis and the controller design.

A. Plant Model

The stability properties of the proposed SV-RC structure are analyzed considering the same plant used for obtaining the experimental results presented in the next section. The control structure is applied for regulating the currents in a three-phase APF, as shown in Fig. 12. The plant has the inverter voltage vector as input, the RL filter current vector as output and the voltage vector at the PCC ($\vec{v}_p$) as an output disturbance. Thus, the transfer function of the plant in s-domain is

$$G_p(s) = \frac{\vec{i}_f}{\vec{d}} = \frac{\frac{V_{dc}}{R_f}}{1 + \frac{L_f}{R_f}s}, \tag{10}$$

where $\vec{d}$ is the space-vector obtained from the duty cycles.

The parameter L_f was determined during the converter design in order to comply with the maximum admissible output current ripple. Considering a rated phase current of 10 A_{rms}, a maximum ripple of 10%, DC-link voltage of 500 V, grid rated voltage of 127 V and switching frequency of 18 kHz, the value of $L_f = 3.5$ mH was obtained. After building the inductor, the value of $R_f = 150$ mΩ was measured.

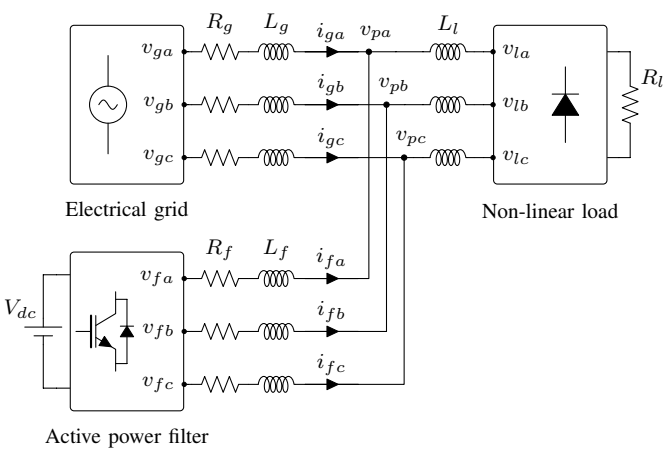

Figure 12. Diagram of the APF used for evaluating the proposed SV-RC.

B. Increasing the Stability Domain

Since the modeled plant has nonzero relative degree, its stability domain must be enlarged in order to enclose the Nyquist diagram of the plant. For this reason, it is recommended to include a low-pass filter (LPF) in the RC structure [18]. The LPF must have DC gain equal to one and cutoff frequency chosen based on the maximum frequency the controller should be able to regulate. In the application exemplified in this paper, the cutoff frequency is $f_c = 1.8$ kHz, which corresponds to the 30th harmonic component.

Most types of LPF provoke not only attenuation but also different phase angle displacements on the input vector harmonic components. The magnitude attenuation of high order harmonic components is desirable for improving stability. However, phase angle displacements modify the frequencies in which the controller poles occur. In this paper, a finite impulse response (FIR) filter of order L was chosen due to its linear phase displacement characteristic, which can be adequately compensated by adjusting the controller parameter i_d, as described in the Appendix.

According to the Appendix and considering that i'_d must be an integer, the order of the FIR filter must be even. Some authors use a FIR filter with $L = 2$ in order to achieve a low impact on the controller poles displacement [12] [19]. However, since the filter presented in the Appendix allows for compensating for this effect, higher order filters could be used for greater attenuation of high order harmonic components. Thus, a filter with $L = 6$ was used, without loss of performance, for all RC-based controllers implemented here.

The iGDSC controller and the SV-RC proposed in [15] have their stability properties analyzed below in more detail. The block diagram of the control system in complex notation, using the iGDSC controller, is shown in Fig. 13. The controller is represented inside the dashed rectangle, including the gain k_{rc} and the LPF in the feedback path ($Q(z)$). As it will be shown later, the unit time computational delay $\left(z^{-1}\right)$ has a significant impact on the system stability. A lead compensator (H_l) is then introduced in order to minimize this effect, through a phase angle advance. Fig. 14 illustrates how the iGDSC controller can be implemented, with real and imaginary parts separated.

0278-0046 (c) 2018 IEEE. Personal use is permitted, but republication/redistribution requires IEEE permission. See http://www.ieee.org/publications_standards/publications/rights/index.html for more information.

This article has been accepted for publication in a future issue of this journal, but has not been fully edited. Content may change prior to final publication. Citation information: DOI 10.1109/TIE.2018.2847661, IEEE Transactions on Industrial Electronics

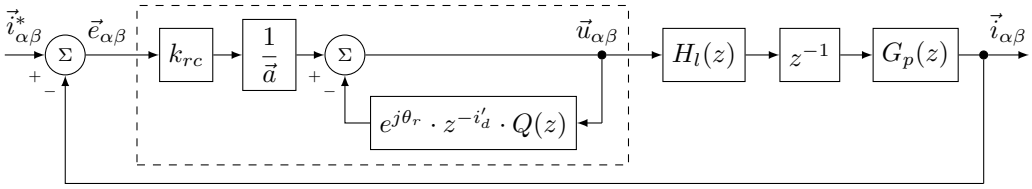

Figure 13. Block diagram of the analyzed system in complex notation using the proposed SV-RC (iGDSC), with LPF and lead compensator.

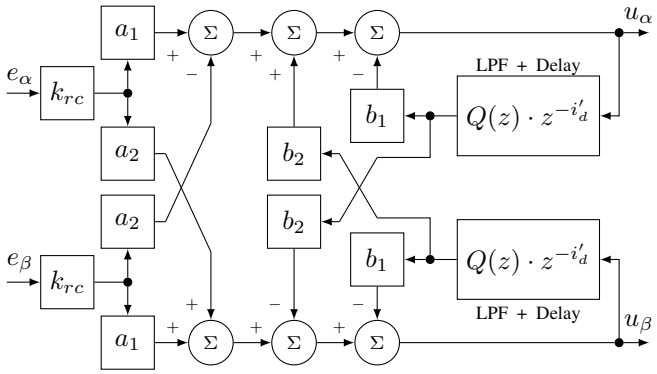

Figure 14. Block diagram of iGDSC-based controller using scalar notation, with gain k_{rc} and LPF $Q(z)$. $a_1 = real\,(\vec{a}^{-1})$, $a_2 = imag\,(\vec{a}^{-1})$, $b_1 = real\,(e^{-j\theta_r})$ and $b_2 = imag\,(e^{-j\theta_r})$.

A stability evaluation using only Bode diagram and phase margin has some limitations for systems having multiple resonant frequencies and multiple 0 dB gain or $-180°$ phase crossing frequencies [20]. In such cases, another relative stability indicator that can be used to evaluate the proximity to instability is the minimum distance η between the Nyquist trajectory and the critical point $(-1 + j0)$. The inverse of this parameter is known as the sensitivity peak. The Nyquist diagrams of the systems considering the iGDSC controller and the SV-RC proposed in [15], using the same FIR filter and gain k_{rc}, are shown in Figs. 15 and 16, respectively. The minimum distances to the critical point confirm the better stability properties of the system having the iGDSC controller. For this reason, the procedures for choosing the design parameters in the case study are detailed only for the proposed iGDSC controller.

C. Design Methodology

Since the sensitivity function can also be used for discrete-time systems and the proposed SV-RC is a digital controller, it is useful to discretize the plant. $G_p(z)$ and the unit time computational delay (z^{-1}) represent the plant transfer function in the discrete-time domain. The zero-order hold (ZOH) discretization method is used in order to take into account the inherent half-sample delay of the PWM [20].

As shown in Fig. 15, the resonance peaks of the proposed SV-RC are represented in the Nyquist diagram of the OLTF as multiple circumferences. These resonance peaks generate several crossover frequencies, making it difficult to tune the SV-RC gain using gain and phase margins. Besides that, these margins have negative correlation (Fig. 15). Thus, the indicator η is used to evaluate relative stability.

The effect of the unit time computational delay may be mitigated via a phase compensation $(H_l(z))$ implemented

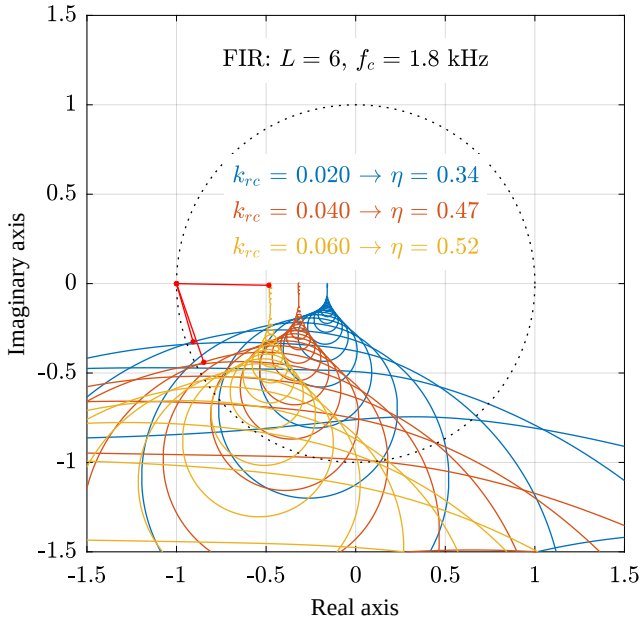

Figure 15. Nyquist diagram of the open-loop system using the iGDSC controller proposed in this paper, with FIR filter $Q(z)$.

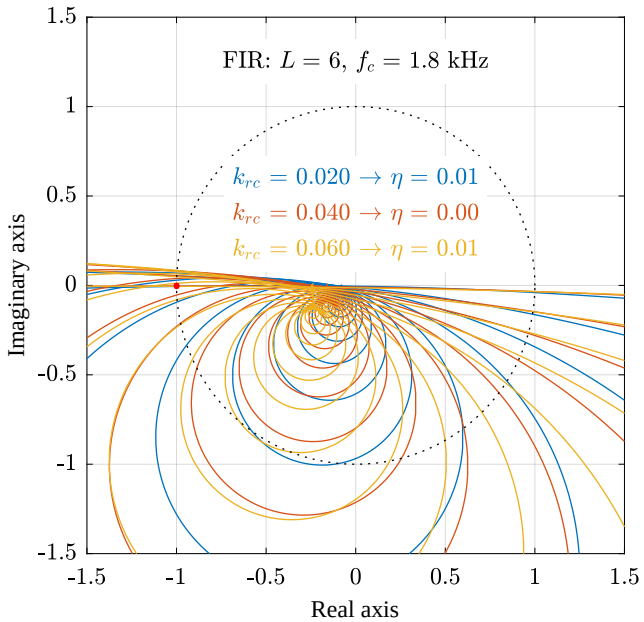

Figure 16. Nyquist diagram of the open-loop system using the SV-RC proposed in [15], with FIR filter $Q(z)$.

along with the SV-RC. For clarity purposes, the system without considering the unit time computational delay and lead compensator $H_l(z)$ will be called "system without delay" (*swd*); the system considering only the delay, but not the lead compensator will be called "uncompensated system" (*us*); and

0278-0046 (c) 2018 IEEE. Personal use is permitted, but republication/redistribution requires IEEE permission. See http://www.ieee.org/publications_standards/publications/rights/index.html for more information.

This article has been accepted for publication in a future issue of this journal, but has not been fully edited. Content may change prior to final publication. Citation information: DOI 10.1109/TIE.2018.2847661, IEEE Transactions on Industrial Electronics

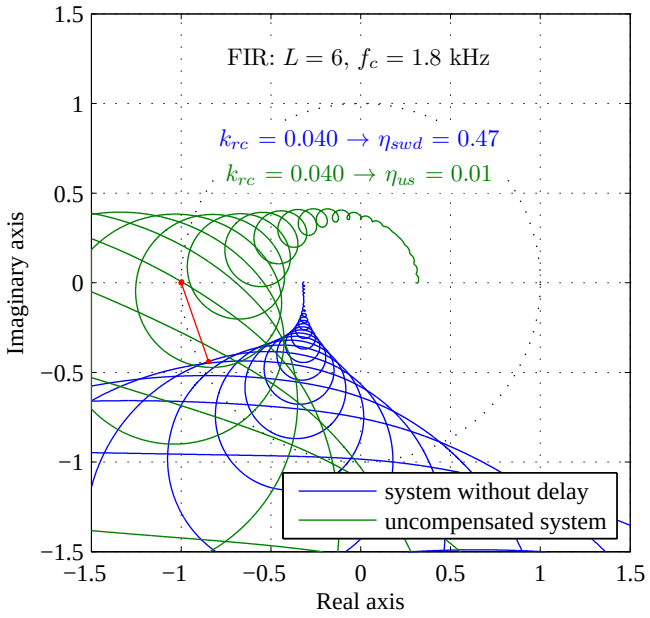

Figure 17. Nyquist diagrams of the open-loop system using iGDSC controller with and without the effect of z^{-1}.

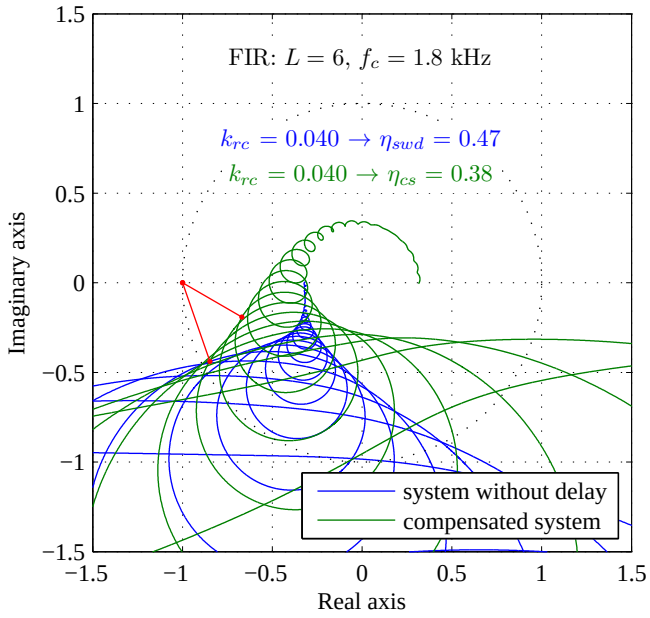

Figure 18. Nyquist diagrams of the open-loop system using iGDSC controller without the effect of z^{-1} and of the "compensated system".

the system with both delay and lead compensator will be called "compensated system" (cs).

Thus, the iGDSC controller gain tuning and the lead compensator design can be done through the following eight steps:

- **Step 1:** Considering the "system without delay", k_{rc} is tuned to obtain the greatest η_{swd}. For the considered $G_p(z)$, $k_{rc} = 0.055$ results in maximum η_{swd}.
- **Step 2:** In order to evaluate some possible operating conditions of the "system without delay", other k_{rc} gains should be selected around the k_{rc} obtained in Step 1. All considered values of k_{rc} are represented in the first column of Table II.
- **Step 3:** For each selected k_{rc}, Table II is filled with the following data of the "system without delay": phase margin PM_{swd}, critical gain crossover frequency f_{PM_swd} and relative stability indicator η_{swd}.

Table II shows the effect of the gain k_{rc} on the closed-loop stability of the "system without delay" using the iGDSC controller. It can be observed from η_{swd} in Table II that although the phase margin still increases for gains higher than 0.055, the system becomes nearer to the critical point and therefore is less stable.

By adding the unit time computational delay z^{-1} along with $G_p(z)$, the system becomes unstable for all evaluated k_{rc}. Fig. 17 shows the Nyquist diagrams of the control system with and without this effect for $k_{rc} = 0.040$. These diagrams clearly show that the delay must be compensated, since it may cause instability. For this, a lead compensator is suggested:

$$H_l(s) = \frac{s+Z}{s+P}, \tag{11}$$

in which $Z < P$.

At this point, the designer must compute the phase angle of the OLTF of the "uncompensated system" at the frequency f_{PM_swd} ($\angle OLTF_{us}(j2\pi f_{PM\_swd})$). The sum of this phase angle with $180°$ is here referred to as ϕ_{us}, and it represents the minimum phase angle of the lead compensator.

- **Step 4:** Considering the "uncompensated system", the parameter ϕ_{us} is calculated by

$$\phi_{us} = \angle OLTF_{us}(j2\pi f_{PM\_swd}) + 180°. \tag{12}$$

For each selected k_{rc}, the ϕ_{us} is shown in the last column of Table II.

- **Step 5:** The designer should select the phase lead ψ that will be applied to the "uncompensated system". The objective is to mitigate the effect of the unit time computational delay on the system stability, making $PM_{cs} \approx PM_{swd}$. For this,

$$\psi = PM_{swd} - \phi_{us}. \tag{13}$$

Thus, by considering the operating condition represented in the first line of Table II, the designed lead compensator should lead $\psi = PM_{swd} - \phi_{us} = 30.7°$ at the frequency $f_{PM\_swd} = 1.54$ kHz.

This strategy does not guarantee that the "compensated system" will have the same critical gain crossover frequency of the "system without delay". However, it allows the designer to use a fixed frequency (f_{PM_swd}) to aid in tuning the lead compensator. For this reason, the choice of the controller parameters must be based on the stability properties and critical crossing frequency of the "compensated system".

- **Step 6:** The lead compensator is discretized. In this paper, Tustin's method was used for this discretization.

A new table (Table III) is constructed for the "compensated system" as explained below. Each line of this table corresponds to a line in Table II.

- **Step 7:** For each selected k_{rc}, Table III is filled with the following data of the "compensated system": phase

0278-0046 (c) 2018 IEEE. Personal use is permitted, but republication/redistribution requires IEEE permission. See http://www.ieee.org/publications_standards/publications/rights/index.html for more information.

This article has been accepted for publication in a future issue of this journal, but has not been fully edited. Content may change prior to final publication. Citation information: DOI 10.1109/TIE.2018.2847661, IEEE Transactions on Industrial Electronics

Table II
EFFECTS OF THE IGDSC CONTROLLER GAIN k_{rc} ON THE "SYSTEM WITHOUT DELAY".

FIR: $L = 6$, $f_c = 1.8$ kHz				
k_{rc}	PM_{swd}	f_{PM_swd}	η_{swd}	ϕ_{us}
0.020	19.6°	1.54 kHz	0.338	-11.1°
0.025	21.1°	1.55 kHz	0.366	-9.9°
0.030	23.6°	1.91 kHz	0.407	-14.5°
0.035	24.9°	1.92 kHz	0.431	-13.4°
0.040	27.0°	1.93 kHz	0.465	-11.5°
0.045	28.2°	2.28 kHz	0.487	-17.5°
0.050	30.0°	2.29 kHz	0.515	-15.9°
0.055	31.0°	2.65 kHz	0.535	-22.0°
0.060	32.4°	3.01 kHz	0.516	-27.8°

Table III
PARAMETERS OF THE IGDSC CONTROLLER AND THEIR EFFECT ON THE "COMPENSATED SYSTEM".

FIR: $L = 6$, $f_c = 1.8$ kHz						
k_{rc}	PM_{cs}	f_{PM_cs}	h_{PM_cs}	η_{cs}	Z	P
0.020	22.2°	1.16kHz	19	0.374	5.49e3	1.70e4
0.025	21.4°	1.52kHz	25	0.345	5.51e3	1.72e4
0.030	26.8°	0.81kHz	13	0.457	5.83e3	2.46e4
0.035	27.4°	1.17kHz	19	0.432	5.83e3	2.49e4
0.040	27.0°	1.89kHz	31	0.382	5.83e3	2.51e4
0.045	30.8°	0.81kHz	13	0.497	5.84e3	3.52e4
0.050	32.1°	0.82kHz	13	0.449	5.84e3	3.55e4
0.055	32.7°	0.46kHz	7	0.549	5.57e3	4.98e4
0.060	30.7°	0.45kHz	7	0.529	5.03e3	7.11e4

margin PM_{cs}, critical gain crossover frequency f_{PM_cs} and relative stability indicator η_{cs}.

- **Step 8:** Finally, the most appropriate operating condition for the design is chosen. Fig. 18 shows the Nyquist diagrams of the "uncompensated system" and "compensated system" for $k_{rc} = 0.040$.

The higher the phase lead ψ, the higher its influence on system performance. Thus, there is a trade-off between relative stability and performance. It is advisable to evaluate the stability margins of the "compensated system" (through phase margin and indicator η) and also the maximum frequency the controller can regulate in order to choose the parameters of the compensator. Since similar stability margins were obtained, the choice can be based on the largest bandwidth achieved, represented in terms of harmonic components by h_{PM_cs}.

In the example presented in this paper, the chosen gain was $k_{rc} = 0.040$, which results in a "compensated system" with phase margin of approximately 27° and critical gain crossing frequency corresponding to the 31st harmonic component. This operating condition is highlighted in Table III.

IV. EXPERIMENTAL RESULTS

A prototype of a system with a three-phase APF as shown in Fig. 12 was built for the experimental verification of the proposed SV-RC. The prototype is shown in Fig. 19 and its parameters are indicated in Table IV. The load currents' space-vector has the harmonic spectrum shown in Fig. 2. For this reason, the only harmonic components that need to be regulated are those in the family ($6k + 1$, $k \in \mathbb{Z}$). If the load currents had additional components, after the harmonic spectrum analysis, the designer should select an additional controller to operate in parallel with the iGDSC. For example, considering an unbalanced load such that harmonics of the currents' space-vector were in the family ($6k \pm 1$, $k \in \mathbb{Z}$), two iGDSC tuned for regulating the components in ($6k + 1$, $k \in \mathbb{Z}$) and ($6k - 1$, $k \in \mathbb{Z}$) could be used in parallel. Since they would be in parallel, the expected response time would be similar to the one obtained using only one iGDSC, i. e., faster than $nk \pm m$ RCs.

The phase-a grid, load and APF output currents (i_{ga}, i_{la} and i_{fa}, respectively) during the control startup are shown in Fig. 20. As expected, the APF injects the necessary harmonic components to make the grid current approximately sinusoidal. The harmonic spectra of the load and grid currents are shown in Fig. 21 and Fig. 22, respectively. All components for which the SV-RC was designed were significantly reduced. Moreover, the THD-F, with respect to the fundamental-frequency component, was reduced from 25.3% to 3.64%.

Fig. 23 shows the response of the control system to a load step change. As expected, the grid compensated current i_{ga} remains approximately sinusoidal. It can also be observed that the APF output current i_{fa} accurately tracks its reference.

Table V shows a performance comparison between controllers based on P-SSIs in parallel [6], $6k \pm 1$ RC [14] in parallel with a proportional action (P), $6k \pm 1$ RC implemented in a plug-in configuration [11], $6k+1$ SV-RC proposed in [15] and the iGDSC controller.

All control strategies were evaluated under the same experimental conditions. The P-SSIs were designed using the discretization method "Tustin with pre-warping" and individual compensation of the computational delay for each SSI, as

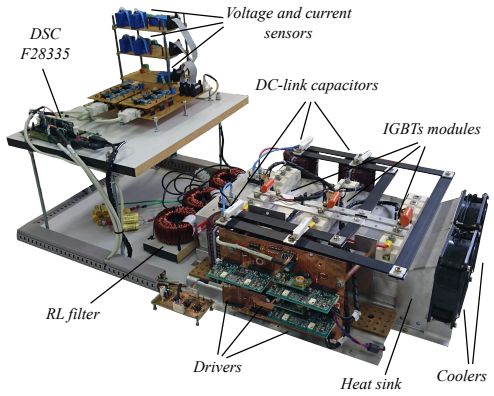

Figure 19. Prototype used to validate the iGDSC controller.

Table IV
PARAMETERS OF EXPERIMENTAL PROTOTYPE.

R_f (mΩ)	L_f (mH)	R_l (Ω)	L_l (mH)	V_{dc} (V)	$V_{g(l-l)}$ (V_{rms})	f_s (kHz)	f_{sw} (kHz)
150	3.5	24.4	1.0	500	127	18	18

0278-0046 (c) 2018 IEEE. Personal use is permitted, but republication/redistribution requires IEEE permission. See http://www.ieee.org/publications_standards/publications/rights/index.html for more information.

This article has been accepted for publication in a future issue of this journal, but has not been fully edited. Content may change prior to final publication. Citation information: DOI 10.1109/TIE.2018.2847661, IEEE Transactions on Industrial Electronics

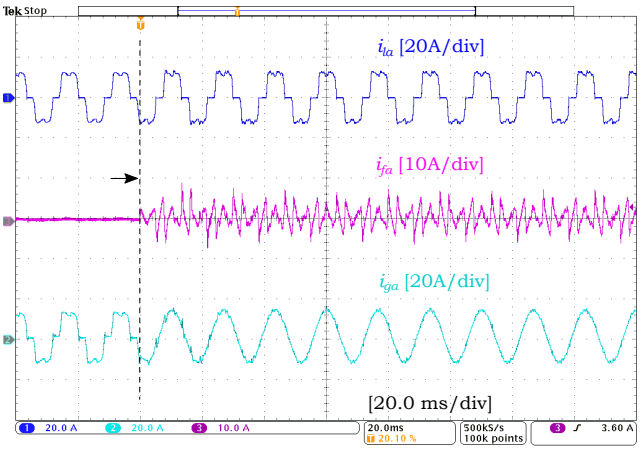

Figure 20. Phase-*a* grid, load and APF output currents during control startup.

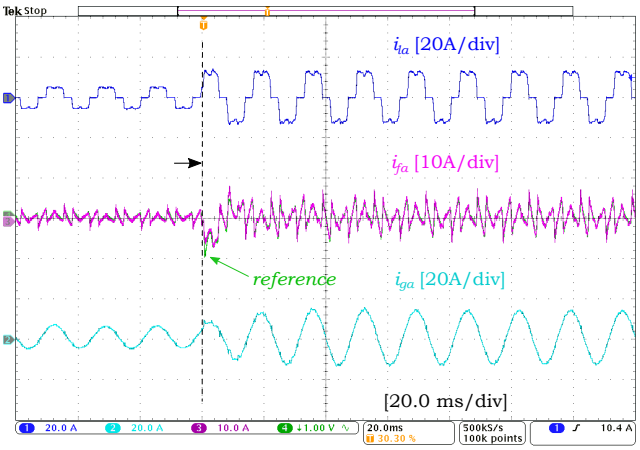

Figure 23. Phase-*a* load, APF output (reference and measured) and grid currents for a load step change.

Harmonics

THD−F	25.3 %			
THD−R	24.5 %			
RMS	8.93 A			
	Freq (Hz)	Mag (%)	Mag RMS (A)	Phase (°)
1	60.00	100	8.64	0.000
3	180.0	484m	41.8m	179.1
5	300.0	22.2	1.92	173.4
7	420.0	8.77	757m	153.8
9	540.0	201m	17.4m	−20.55
11	660.0	6.21	536m	−39.53
13	780.0	3.29	284m	−36.87
15	900.0	119m	10.3m	62.94
17	1.020k	2.50	216m	74.83
19	1.140k	1.42	123m	98.00

Use 'Harmonics → Display → Select' to select a harmonic

Figure 21. Harmonic spectrum of the phase-*a* load current.

Harmonics

THD−F	3.64 %			
THD−R	3.60 %			
RMS	8.94 A			
	Freq (Hz)	Mag (%)	Mag RMS (A)	Phase (°)
1	60.00	100	8.85	0.000
3	180.0	46.7m	4.13m	136.4
5	300.0	1.06	94.0m	92.77
7	420.0	535m	47.3m	82.68
9	540.0	266m	23.5m	−14.25
11	660.0	202m	17.9m	66.33
13	780.0	95.6m	8.46m	28.17
15	900.0	333m	29.5m	130.0
17	1.020k	765m	67.7m	−122.6
19	1.140k	123m	10.9m	−111.0

Use 'Harmonics → Display → Select' to select a harmonic

Figure 22. Harmonic spectrum of the phase-*a* grid current during the APF steady state operation.

in [21]. The $6k \pm 1$ RCs proposed in [14] and [11], as well as the $6k + 1$ SV-RC in [15], were implemented using the same LPF $Q(z)$ and lead compensator $H_l(z)$ used for the iGDSC controller. However, since the solutions proposed in [14] and [15] resulted in instability, a proportional action was used in parallel. In order to provide a fair comparison, all controllers' gains (k_p and k_{rc}) were tuned for achieving similar PM and

Table V
COMPARISON OF CONTROLLERS' PERFORMANCE.

Control strategy	k_p	k_{rc}	PM †	η †	ST (ms)	VTHD
P-SSIs [6]	0.08	3.8‡	26.8°	0.30	89	3.45%
$6k \pm 1$ RC [14]	0.04	0.038	27.3°	0.34	50	3.43%
$6k \pm 1$ RC [11]	0.06	0.045	27.0°	0.33	146	4.35%
$6k + 1$ SV-RC [15]	0.05	0.036	27.0°	0.33	43	3.68%
$6k + 1$ iGDSC	–	0.040	27.0°	0.38	26	2.51%

† Obtained during the design procedure using Matlab; ‡ Integral gain.

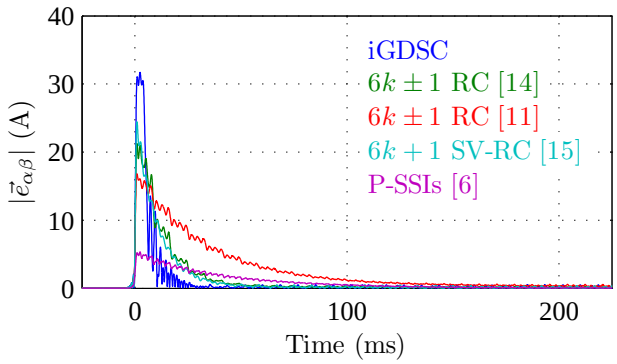

Figure 24. Absolute value of the error space-vector for each control strategy.

f_{PM}. If the same gains were chosen for all controllers, the relative stability of the strategies proposed in [14], [11] and [15] would be strongly reduced.

The parameters chosen for the comparison were the stability margin (η); the settling time (ST), defined as the time interval from the moment the controller is enabled until the error absolute value becomes smaller than 5% of the fundamental component amplitude; and the vector THD (VTHD) [22] up to the 50th harmonic component. The proposed controller led to higher η, lower ST and lower VTHD. The absolute value of the error space-vector for each implemented control strategy, used for computing the settling times, is shown in Fig. 24. Since the proposed controller has the largest stability domain ($a(s) = 1$), it allows the application of the RC in a single direct path, different from the other RC structures, which use additional proportional action in order to improve stability.

0278-0046 (c) 2018 IEEE. Personal use is permitted, but republication/redistribution requires IEEE permission. See http://www.ieee.org/publications_standards/publications/rights/index.html for more information.

This article has been accepted for publication in a future issue of this journal, but has not been fully edited. Content may change prior to final publication. Citation information: DOI 10.1109/TIE.2018.2847661, IEEE Transactions on Industrial Electronics

V. Conclusion

The paper presents a new SV-RC able to regulate different positive- and negative-sequence vector harmonic components. As a consequence, a reduced response time is achieved, in comparison with RC implemented in the phase quantities or in the α and β components of the error signals. A stability analysis is performed showing that the proposed SV-RC has better stability properties than the previous SV-RC. A procedure for designing the SV-RC gain and a lead compensator for the unit time computational delay were also proposed, based on phase margin and sensitivity function analysis. Experiments were performed in order to support the theoretical analysis and validate the SV-RC applied in a prototype with a three-phase APF. In comparison with P-SSIs and $6k \pm 1$ RC and the previous $6k + 1$ SV-RC, the proposed controller showed lower settling time and total harmonic distortion.

Appendix

Consider a FIR filter with symmetric coefficients

$$Q(z) = b_0 + b_1 z^{-1} + \cdots + b_{\frac{L}{2}} z^{-\frac{L}{2}} + \cdots + b_1 z^{-(L-1)} + b_0 z^{-L}, \tag{14}$$

in which L is an even number.

Since a harmonic vector component has constant magnitude and rotates at speed $h\omega_1$, its phase angle displacement during one sampling interval is $(2\pi/N)h$. Thus, the gain of the FIR filter for a harmonic input vector can be easily shown to be equal to

$$\vec{G}^{(h)}_{Q(z)} = \left[b_{\frac{L}{2}} + \sum_{l=0}^{\frac{L}{2}-1} 2b_l \cos\left(\frac{2\pi}{N} \frac{L-2l}{2} h \right) \right] e^{-jh\frac{2\pi}{N}\frac{L}{2}}. \tag{15}$$

The term z^{-i_d} of iGDSC also produces a linear phase angle displacement, whose value determines the set of harmonic components to be controlled, i. e., the poles of the controller. Thus, the parameter i_d can be altered in order to compensate for the phase error caused by the FIR filter and, as a consequence, to preserve the frequencies where the controller poles occur. The corrected parameter can be calculated as follows. Let $-h\theta_d$ and $-h\theta'_d$ be the phase angle displacements caused by the terms z^{-i_d} and $z^{-i'_d}$, of the originally designed and compensated iGDSC controllers, respectively. Since $-h(2\pi/N)(L/2)$ is the phase angle displacement caused by Q(z), $h\theta'_d$ must be equal to

$$h\theta'_d = h\theta_d - h\frac{2\pi}{N}\frac{L}{2} \Rightarrow \theta'_d = \theta_d - \frac{2\pi}{N}\frac{L}{2}. \tag{16}$$

Thus,

$$i'_d = \frac{N}{2\pi}\theta'_d \Rightarrow i'_d = i_d - \frac{L}{2}. \tag{17}$$

References

[1] S. Bhattacharya, T. M. Frank, D. M. Divan, and B. Banerjee, "Parallel active filter system implementation and design issues for utility interface of adjustable speed drive systems," in *Thirty-First IAS Annual Meeting, IEEE*, vol. 2, pp. 1032–1039, Oct. 1996.

[2] L. R. Limongi, R. Bojoi, G. Griva, and A. Tenconi, "Digital current-control schemes," *IEEE Ind. Electron. Magazine*, vol. 3, no. 1, pp. 20–31, Mar. 2009.

[3] M. Bojrup, P. Karlsson, M. Alaküla, and L. Gertmar, "A multiple rotating integrator controller for active filters," in *EPE Conf. Proc.*, 1999.

[4] D. N. Zmood and D. G. Holmes, "Stationary frame current regulation of PWM inverters with zero steady state error," in *30th Annual IEEE PESC*, vol. 2, pp. 1185–1190, 1999.

[5] A. Rodríguez, C. Girón, M. Rizo, V. Sáez, E. Bueno, and F. J. Rodríguez, "Comparison of current controllers based on repetitive-based control and second order generalized integrators for active power filters," in *35th Annual Conf. of IEEE Ind. Electron.*, pp. 3223–3228, 2009.

[6] X. Yuan, W. Merk, H. Stemmler, and J. Allmeling, "Stationary-frame generalized integrators for current control of active power filters with zero steady-state error for current harmonics of concern under unbalanced and distorted operating conditions," *IEEE Trans. Ind. App.*, vol. 38, no. 2, pp. 523–532, Mar. 2002.

[7] C. A. Busada, S. G. Jorge, A. E. Leon, and J. A. Solsona, "Current controller based on reduced order generalized integrators for distributed generation systems," *IEEE Trans. Ind. Electron.*, vol. 59, no. 7, pp. 2898–2909, Jul. 2012.

[8] F. A. S. Neves, M. A. C. Arcanjo, G. M. S. Azevedo, H. E. P. de Souza, and L. T. L. Viltre, "The SVFT-based control," *IEEE Trans. Ind. Electron.*, vol. 61, no. 8, pp. 4152–4160, Aug. 2014.

[9] P. Mattavelli and F. P. Marafao, "Repetitive-based control for selective harmonic compensation in active power filters," *IEEE Trans. Ind. Electron.*, vol. 51, no. 5, pp. 1018–1024, Oct. 2004.

[10] S. Hara, T. Omata, and M. Nakano, "Synthesis of repetitive control systems and its application," in *Proc. of IEEE 24th Conf. on Decision and Control*, pp. 1387–1392, Fort Lauderdale, USA, 1985.

[11] W. Lu, K. Zhou, D. Wang, and M. Cheng, "A generic digital nk ± m-order harmonic repetitive control scheme for PWM converters," *IEEE Trans. Ind. Electron.*, vol. 61, no. 3, pp. 1516–1527, Mar. 2014.

[12] K. Zhou, K.-S. Low, D. Wang, F.-L. Luo, B. Zhang, and Y. Wang, "Zero-phase odd-harmonic repetitive controller for a single-phase PWM inverter," *IEEE Trans. Power Electron.*, vol. 21, no. 1, pp. 193–201, Jan. 2006.

[13] G. Escobar, P. G. Hernandez-Briones, P. R. Martinez, M. Hernandez-Gomez, and R. E. Torres-Olguin, "A repetitive-based controller for the compensation of $6\ell \pm 1$ harmonic components," *IEEE Trans. Ind. Electron.*, vol. 55, no. 8, pp. 3150–3158, Aug. 2008.

[14] W. Lu and K. Zhou, "A novel repetitive controller for nk ± m order harmonics compensation," in *Proc. of the 30th Chinese Control Conf.*, pp. 2480–2484, Jul. 2011.

[15] Z. Luo, M. Su, J. Yang, Y. Sun, X. Hou, and J. M. Guerrero, "A repetitive control scheme aimed at compensating the 6k + 1 harmonics for a three-phase hybrid active filter," *Energies*, vol. 9, no. 10, p. 787, Sep. 2016.

[16] F. A. S. Neves, M. C. Cavalcanti, H. E. P. de Souza, F. Bradaschia, E. J. Bueno, and M. Rizo, "A generalized delayed signal cancellation method for detecting fundamental-frequency positive-sequence three-phase signals," *IEEE Trans. Power Del.*, vol. 25, no. 3, pp. 1816–1825, Jul. 2010.

[17] B. Francis and W. Wonham, "The internal model principle for linear multivariable regulators," *Applied Mathematics and Optimization*, vol. 2, no. 2, pp. 170–194, Jun. 1975.

[18] S. Hara, Y. Yamamoto, T. Omata, and M. Nakano, "Repetitive control system: a new type servo system for periodic exogenous signals," *IEEE Trans. Automatic Control*, vol. 33, no. 7, pp. 659–668, Jul. 1988.

[19] B. Zhang, D. Wang, K. Zhou, and Y. Wang, "Linear phase lead compensation repetitive control of a cvcf pwm inverter," *IEEE Trans. Ind. Electron.*, vol. 55, no. 4, pp. 1595–1602, Apr. 2008.

[20] A. G. Yepes, F. D. Freijedo, . Lopez, and J. Doval-Gandoy, "Analysis and design of resonant current controllers for voltage-source converters by means of nyquist diagrams and sensitivity function," *IEEE Trans. Ind. Electron.*, vol. 58, no. 11, pp. 5231–5250, Nov. 2011.

[21] A. G. Yepes, F. D. Freijedo, J. Doval-Gandoy, . López, J. Malvar, and P. Fernandez-Comesaña, "Effects of discretization methods on the performance of resonant controllers," *IEEE Trans. Power Electron.*, vol. 25, no. 7, pp. 1692–1712, Jul. 2010.

[22] F. A. S. Neves, H. E. P. de Souza, M. C. Cavalcanti, F. Bradaschia, and E. J. Bueno, "Digital filters for fast harmonic sequence component separation of unbalanced and distorted three-phase signals," *IEEE Trans. Ind. Electron.*, vol. 59, no. 10, pp. 3847–3859, Oct. 2012.

0278-0046 (c) 2018 IEEE. Personal use is permitted, but republication/redistribution requires IEEE permission. See http://www.ieee.org/publications_standards/publications/rights/index.html for more information.

This article has been accepted for publication in a future issue of this journal, but has not been fully edited. Content may change prior to final publication. Citation information: DOI 10.1109/TIE.2018.2847661, IEEE Transactions on Industrial Electronics

Felipe J. Zimann (S'15) was born in Rio do Sul, Brazil, in 1990. He received the B.S and M.Sc. degrees in electrical engineering from the Universidade do Estado de Santa Catarina, Joinville, Brazil, in 2013 and 2016, respectively. He is currently working toward the Ph.D. degree at the same University.

His research interests include power electronics, digital control techniques and power quality.

Mr. Zimann is currently a member of IEEE Industrial Electronics Society and the Brazilian Power Electronic Society.

Rafael C. Neto was born in Cabo de Santo Agostinho, Brazil, in 1991. He received B.S. degree in electronic engineering and M.Sc. degree in electrical engineering from Universidade Federal de Pernambuco, Brazil, in 2016 and 2018, respectively. He was a Visiting Scholar at the Universidade Federal de Santa Maria, Brazil, during 2016.

Since 2018, he has been with the Universidade Federal de Pernambuco, Brazil, where he is a Ph.D. student in electrical engineering. His research interests include power electronics, renewable energy systems and modeling and digital control techniques of static converters.

Mr. Neto is currently a student member of the Brazilian Power Electronic Society (SOBRAEP).

Francisco A. S. Neves (M'00-SM'13) was born in Campina Grande, Brazil, in 1963. He received the B.S. and M.Sc. degrees in electrical engineering from the Universidade Federal de Pernambuco, Recife, Brazil, in 1984 and 1992, respectively, and the Ph.D. degree in electrical engineering from the Universidade Federal de Minas Gerais, Belo Horizonte, Brazil, in 1999. He was a Visiting Scholar at the Georgia Institute of Technology, USA, during 1999, and at the University of Alcala, Spain, from 2008 to 2009.

Since 1993, he has been with the Department of Electrical Engineering, Universidade Federal de Pernambuco, Recife, Brazil, where he is a Professor of electrical engineering. His research interests include power electronics, renewable energy systems, power quality, and grid-connected converters.

Dr. Neves is a co-recipient of The Best Paper Award in two IEEE conferences: International Conference on Power Electronics and Intelligent Control for Energy Conservation in 2005 and International Symposium on Industrial Electronics in 2011.

Helber E. P. de Souza was born in Cabo de Santo Agostinho, Brazil, in 1983. He received the B.S., M.Sc. and Ph.D. degrees in electrical engineering from the Universidade Federal de Pernambuco, Recife, Brazil, in 2006, 2008 and 2012, respectively.

Since 2009 he joined the Department of Industry, Instituto Federal de Educação, Ciência e Tecnologia de Pernambuco, Pesqueira, Brazil. His research interests are power quality, grid synchronization methods and digital control techniques of static converters.

Alessandro L. Batschauer (S'09-M'11) was born in Balneário Camboriú, Brazil, in 1977. He received the B.S.(2000), M.Sc. (2002) and Ph.D (2011) degrees in electrical engineering from Universidade Federal de Santa Catarina (UFSC), Florianópolis-SC, Brazil, in 2000, 2002 and 2011, respectively.

Since 2002, he has been with Department of Electrical Engineering, Universidade do Estado de Santa Catarina. His fields of interest include high-frequency switching converters, power quality, multilevel converters and impedance source converters.

Mr. Batschauer is currently a member of the IEEE TPEL, IEEE TIE and Brazilian Power Electronic Society (SOBRAEP).

Cassiano Rech (S'01-M'06-SM'15) received the B.S., M.Sc., and Ph.D. degrees in electrical engineering from the Universidade Federal de Santa Maria (UFSM), Santa Maria, Brazil, in 1999, 2001, and 2005, respectively.

From 2005 to 2007, he was with the Universidade Regional do Noroeste do Estado do Rio Grande do Sul. From 2008 to 2009, he was with the Universidade do Estado de Santa Catarina (UDESC). Since 2009, he has been with the UFSM, where he is currently a Professor. His research interests include multilevel converters, distributed generation, and modeling and digital control techniques of static converters.

Dr. Rech was the Editor-in-Chief of the Brazilian Power Electronics Journal from 2014 to 2015. From 2016 to 2017, he was the President of the Brazilian Power Electronics Society (SOBRAEP). Since 2018, he has been an Associate Editor of the IEEE Transactions on Industrial Electronics.

0278-0046 (c) 2018 IEEE. Personal use is permitted, but republication/redistribution requires IEEE permission. See http://www.ieee.org/publications_standards/publications/rights/index.html for more information.